

# State-to-state differential cross sections for the reaction $\text{Cl}(^2\text{P}_{3/2}) + \text{CH}_4(\nu_3 = 1, J = 1) \rightarrow \text{HCl}(\nu' = 1, J') + \text{CH}_3$

William R. Simpson, Andrew J. Orr-Ewing and Richard N. Zare

*Department of Chemistry, Stanford University, Stanford, CA 94305, USA*

Received 19 April 1993; in final form 21 May 1993

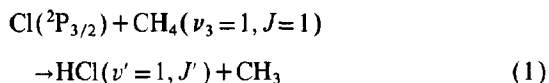
A mixture of methane and chlorine molecules in a helium carrier is expanded into a vacuum chamber using a pulsed valve. Polarized laser photolysis of  $\text{Cl}_2$  at 355 nm is used to produce  $\text{Cl}(^2\text{P}_{3/2})$  with a sharply peaked speed distribution and a known angular distribution. Methane molecules are excited in the asymmetric stretch mode by infrared absorption to the  $\nu_3 = 1, J = 1$  state. Following a 100 ns time delay to allow for reaction,  $\text{HCl}(\nu' = 1, J')$  product molecules are probed by (2+1) resonance-enhanced multiphoton ionization. The resulting photoions are detected with both mass and velocity resolution using a linear time-of-flight mass spectrometer. Application of the methods described by Shafer et al., allows determination of the differential cross section for the specific rovibrational state ionized at a center-of-mass collision energy of 0.159 eV. The time-of-flight data show a change in the product angular distribution with  $J'$  and thus demonstrate the importance of measuring quantum-state-resolved differential cross sections for elucidating the dynamics of this reaction system.

## 1. Introduction

Photolysis of a molecular precursor under bulb conditions to form translationally hot atoms has found widespread application in the study of reaction dynamics [1]. The frequent use of this method results partly from the significant enhancements in signal-to-noise ratios over crossed molecular beam experiments that can be achieved by observing photodissociation-initiated reactions, and partly from the relatively straightforward experimental apparatus required to study reactions in a bulb. Recent developments in the techniques of hot-atom reactions have demonstrated the feasibility of measuring product rotational alignment, second moments of the differential cross section, and other state-resolved vector correlations [2–10] by laser detection methods, particularly laser-induced fluorescence (LIF). In some instances, more detailed information about the form of the differential cross section has been deduced, either by demonstrating stripping-type dynamics from a combination of product energy disposal and velocity projection measurements [6], or by comparing experimental measurements of reaction product velocity distributions with velocity distributions

calculated from assumed forms for the differential cross section [3,8,10]. However, a direct inversion of experimental velocity projection data from a hot-atom reaction to obtain a full differential cross section has not been published.

The preceding Letter [11] has shown that for favorable mass combinations and reaction energetics, complete differential cross sections can be obtained for state-to-state reactions with a translationally hot-atom reagent in a bulb experiment. We illustrate this technique here for the reaction



at a center-of-mass collision energy of 0.159 eV (1280  $\text{cm}^{-1}$ ). This low collision energy restricts the study to reaction within at most 0.093 eV (750  $\text{cm}^{-1}$ ) of the barrier, and hence we anticipate that the observed dynamics will reflect the nature of the potential-energy surface close to the minimum-energy pathway. The angular distribution of the HCl product is determined from laboratory-frame projections of its velocity distribution. By state selecting the  $\text{CH}_4$  reagent, we are able to reduce the averaging over ini-

tial states. In addition, the use of infrared radiation to excite reagents vibrationally affords control of the rotational and vibrational states of the reagent and thus provides the opportunity to study the effects of these motions on the reactivity and dynamics. In this and other laboratories [12–15] previous experiments have shown that vibrational energy can have a profound influence on chemical reactivity, even for low levels of vibrational excitation, but the role of the reagent internal modes on the differential cross section has not been explored.

The reaction of Cl with ground state  $\text{CH}_4$  is nearly thermoneutral; it has an endothermicity of  $0.082 \pm 0.004$  eV ( $661 \pm 35$   $\text{cm}^{-1}$ ) and a barrier of  $\approx 0.152$  eV ( $1220$   $\text{cm}^{-1}$ ) [16]. A quantum-mechanical calculation of the transition-state energy and structure has been performed by Truong et al. [17], who predict a linear transition state. Although past work on this system is sparse, this system is energetically and kinematically similar to that of  $\text{O}(^3\text{P}) + \text{hydrocarbons}$  studied by Andresen and Luntz [18]. In these reactions, the observed cold OH rotational distributions were interpreted to be a result of OH back scattering from a linear transition state. By measuring the differential cross section for reaction (1) directly, we avoid having to draw inferences about the nature of the reactive scattering from product rotational-state population distributions alone. The data we present here demonstrate that cold rotational distributions are not necessarily indicative of backward scattering of products.

## 2. Experimental

The experimental apparatus is shown schematically in fig. 1. It consists of a reaction chamber and a differentially pumped detection chamber. Reagents are expanded via a pulsed nozzle into the reaction chamber, where they are intersected by the photolysis and infrared pumping laser beams. Products are ionized by the probe laser, and ions are extracted through a slit into the detection chamber, where they are detected by a chevron microchannel plate particle multiplier. The reaction chamber is typically operated at pressures  $< 3 \times 10^{-5}$  Torr, and the detection chamber is maintained at  $< 6 \times 10^{-7}$  Torr.

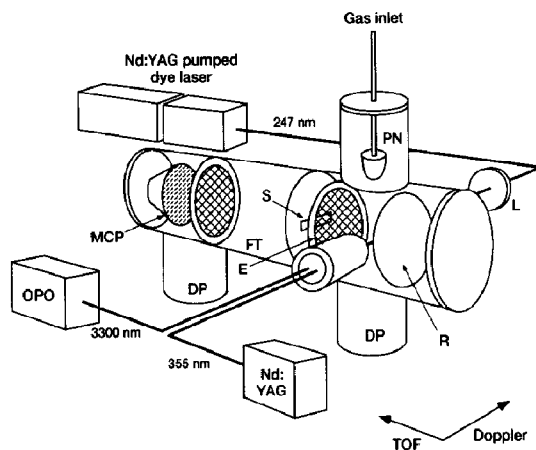


Fig. 1. Schematic diagram of the experimental apparatus. The two axes along which velocity resolution can be obtained are shown at bottom right. The abbreviations used are: PN pulsed nozzle, L lens, DP diffusion pump, OPO optical parametric oscillator, MCP microchannel plates, E extractor plate, R repeller plate, S slit, FT flight tube.

Chlorine atoms are generated by photolysis of  $\text{Cl}_2$  at 355 nm (50 mJ in a 1 mm diameter spot), and the ultraviolet radiation is made by frequency tripling a Nd:YAG laser (Quantel YG-581-20). At this wavelength, the photodissociation produces almost exclusively (98%)  $\text{Cl}(^2\text{P}_{3/2})$ , with an anisotropy parameter  $\beta = -1$  [19,20]. Relative motion of the  $\text{Cl}_2$  and  $\text{CH}_4$  molecules is reduced by coexpanding a mixture of 4%  $\text{Cl}_2$ , 40%  $\text{CH}_4$ , and 56% He, total pressure 500 Torr, through a pulsed nozzle. Cooling in the expansion produces an effective translational temperature lower than the rotational temperature of HCl impurity in the mix, which is measured to be about 15 K. Using this upper limit to the translational temperature, the spread in collision energies about the center of mass is calculated to be less than 0.044 eV fwhm, which is significantly reduced from the 300 K value of 0.196 eV [21].

Methane molecules are excited by infrared absorption on the R(0) line of the fundamental of the  $\nu_3$  mode at  $3030$   $\text{cm}^{-1}$  (3.3  $\mu\text{m}$ ). Pumping the R(0) line results in methane prepared in the A-symmetrized form. The  $\nu_3$  mode of  $\text{CH}_4$  is nominally an asymmetric stretch but also has components of motion orthogonal to the direction of the C–H stretch. The infrared radiation is generated from a lithium niobate optical parametric oscillator (OPO),

pumped by a Nd:YAG laser (Spectra Physics DCR-1). The OPO produces approximately 2 mJ of IR at 3.3  $\mu\text{m}$  and is fired slightly before the photolysis laser (about 10 ns). The IR laser is operated at half the repetition rate of the photolysis and probe lasers. Thus, alternate shots can be subtracted to find the IR-induced signal.

The OPO and photolysis beams copropagate through the chamber to prepare the reagents and initiate reaction. Following a 100 ns reaction time, the products are probed quantum-state specifically by the counterpropagating resonance-enhanced multiphoton ionization (REMPI) laser pulse. Product  $\text{HCl}(v'=1, J')$  molecules are probed by (2+1) REMPI on the (0,1) band of the  $E^1\Sigma^+-X^1\Sigma^+$  transition at about 247 nm [22–25]. Tunable 247 nm light is generated by frequency doubling in a  $\beta$ -barium borate (BBO) crystal, the output of a Nd:YAG-pumped dye laser (Spectra Physics PDL-3 and DCR-2AG) operating on LD489. The probe beam is gently focused with a 500 mm lens into the middle of the region where the molecules were vibrationally excited and photolyzed, which is also the middle of the extraction region of a linear time-of-flight mass spectrometer (TOF-MS). The mass spectrometer signal depends on the mass of the ion formed and the initial velocity of the ion [26–29]. A measurement of the TOF peak shape is equivalent to a one-dimensional projection of the velocities of the ionized molecules along the axis of the TOF tube. The ionization laser has a bandwidth that is smaller than the Doppler width of the product molecules, so only the molecules with a proper Doppler shift to be resonant with the laser are ionized. This Doppler resolution along the probe beam axis can provide a second dimension for velocity projection along an orthogonal axis, but in practice for this system, power broadening limits the available Doppler information. The recording of TOF profiles allows the determination of differential cross sections for this reaction because we can relate the ion signal to the flux of quantum-state resolved product into a solid angle element [11].

Reagent TOF profiles of the  $^{35}\text{Cl}$  mass peak are taken on a fast-digital-sampling oscilloscope (Tektronix TDS 620) by averaging 160 laser shots in 1.5 ns time bins. Reactive TOF profiles of the  $\text{H}^{35}\text{Cl}$  mass peak are taken by averaging 40 laser shots (in 1 ns bins), with the OPO firing and subtracting an av-

erage of 40 laser shots taken with the OPO blocked. This subtraction procedure is repeated many times until the signal-to-noise ratio is acceptable. Typical reactive TOF spectra are the result of 1000 to 4000 laser shots with the OPO on and an equal number of shots with the IR laser off. Between 5 and 50 ions with  $m/z=36$  are formed per laser shot, which is a low enough level to be free from space-charge distortions. The ion signals are found to be independent of total ion yield, which provides additional evidence that space-charge distortion is not a problem. Checks for systematic errors in the subtraction procedure were performed by separately blocking the OPO and photolysis lasers. Blocking the OPO resulted in no difference signal, and blocking the photolysis laser beam resulted in a signal from the energy transfer background described in section 3.3.

### 3. Data and analysis

#### 3.1. $\text{Cl}_2$ photodissociation

A TOF profile for the Cl atoms that arise from the 355 nm photolysis of  $\text{Cl}_2$  is shown in fig. 2. Such profiles were recorded for two reasons: (1) the energetics and anisotropy parameter are known for  $\text{Cl}_2$

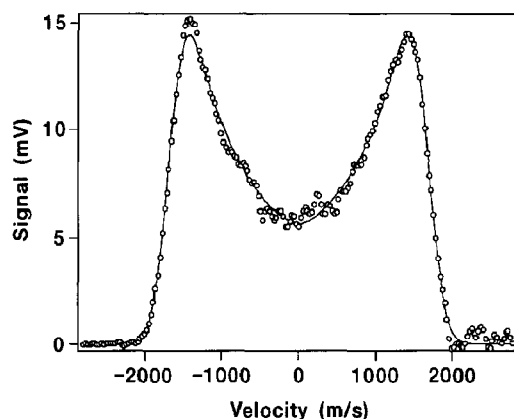


Fig. 2. Experimental TOF profile for Cl atoms from the 355 nm photolysis of  $\text{Cl}_2$ . The polarization of the photolysis laser ( $\epsilon$ ) is perpendicular to the TOF axis. The solid line is a simulation of the TOF profile for  $\beta = -1$  and for a Lorentzian probe laser profile with full width at half maximum 90% of the Doppler width of the Cl atoms.

photolysis at 355 nm, so this signal provides a calibration and check on the instrument. (2) Measurements of the velocity projection as a function of photolysis-probe delay show that negligible flyout occurs on the 100 ns time scale used for the reactive experiments.

Cl atoms are probed by (2+1) REMPI on the  ${}^4P_{3/2}^o \rightarrow {}^2P_{3/2}^o$  transition at 240.53 nm [30]. The double-peaked, symmetric form along the TOF axis is a consequence of the anisotropy of the  $\text{Cl}_2$  photodissociation and the alignment of the electric vector of the linearly polarized photolysis laser ( $\epsilon$ ) perpendicular to the TOF axis. Cl atoms are formed with velocities preferentially perpendicular to  $\epsilon$ , and this velocity distribution is retained immediately after laser ionization. Those  $\text{Cl}^+$  ions with initial velocities antiparallel to the TOF axis are turned around by the repeller plate voltage and reach the detector at a later time than those ions with velocities parallel to this axis. The TOF profile therefore corresponds to a projection of the Cl velocity distribution, which is cylindrically symmetric about  $\epsilon$ , onto the TOF axis, and the peaks in the wings arise because of the "edge-brightening". In section 3.2, we make use of the form of the Cl-atom TOF profile in deducing the nature of the differential cross section for the  $\text{HCl}(v'=1, J')$  product of reaction (1).

### 3.2. Differential cross sections

The purpose of this Letter is to demonstrate the feasibility of measuring state-to-state differential cross sections for a reaction under bulb conditions and to show the importance of such measurements in aiding our understanding of the reaction dynamics. In this section we demonstrate how differential cross section information can be extracted from the experimental TOF profiles. We do note, however, that measurements have also been made in this laboratory of the relative integral cross sections for formation of  $\text{HCl}(v'=1)$  in different rotational states by reaction (1). We observe rotationally cold  $\text{HCl}(v'=1)$ , with essentially no product for  $J' > 4$ . The maximum signal occurs for  $\text{HCl}(v'=1)$  in  $J' = 1$  or 2. Hence, we concentrate on recording differential cross sections for low values of  $J'$ . The observation of rotationally cold  $\text{HCl}(v'=1)$  is significant for our later discussion in section 4.

For reaction (1), we calculate a value of the parameter  $\gamma = u_{\text{AB}}/u$ , defined in the preceding Letter [11], of  $\gamma = 0.325$ . We retain the notation of ref. [11]: specifically  $u_{\text{HCl}}$  is the center-of-mass frame speed of the HCl, and  $u$  is the speed of the center of mass. Reaction (1) therefore lies within a regime approximated by case (3) of ref. [11], i.e. from a measurement of the speed distribution of the product HCl, we can obtain detailed information on the differential cross section. From the known energetics of the state-to-state reaction forming  $\text{HCl}(v'=1, J'=1)$ , the HCl is calculated to have a speed in the center-of-mass frame of  $373 \text{ ms}^{-1}$ , assuming that all the available energy appears in product translation rather than in internal excitation of the  $\text{CH}_3$  radical. Because the speed of the center of mass is  $1147 \text{ m s}^{-1}$ , this energy release will result in a maximum range of HCl laboratory-frame speeds from  $v_{\text{min}} = 774 \text{ m s}^{-1}$  to  $v_{\text{max}} = 1520 \text{ m s}^{-1}$  ( $v_{\text{min}}$  and  $v_{\text{max}}$  are defined in eqs. (11) and (12) of ref. [11]), giving  $v_{\text{range}} = 746 \text{ m s}^{-1}$ . A Newton diagram for reaction (1) conducted under the conditions described in this Letter is shown in fig. 3.

Differential cross sections for reaction (1) were extracted from reactive TOF profiles measured at Doppler line center using the following procedure. First we assumed that the  $\text{CH}_3$  product of the reaction does not contain any internal energy, or that any internal energy present is insignificant compared with the experimental uncertainties. Within this assumption, which we will see is supported by the experimental data, we can use the formalism described in the previous Letter to invert the data to obtain a differential cross section. This data inversion is achieved by expressing the three-dimensional velocity distribution,  $f(v_{\text{HCl}})$ , in terms of its components,  $I_n(v_x, v_y, v_z; u_{\text{HCl}}, \cos \theta_n)$ , corresponding to any scattering angle  $\theta_n$ . Here,  $v_x, v_y, v_z$  denote laboratory-frame HCl velocity components. We start by expanding the normalized differential cross section in terms of scattering angles  $\cos \theta_n$ ,

$$\frac{1}{\sigma} \frac{d\sigma}{d\Omega} = \frac{1}{2\pi} \sum_{n=1}^N a_n \delta(\cos \theta - \cos \theta_n). \quad (2)$$

The weighting coefficients  $a_n$  give a probability for scattering into an angle  $\theta_n$ , and thus give the differential cross section evaluated at  $\cos \theta_n$ . Using the expression in the preceding Letter for the three-di-

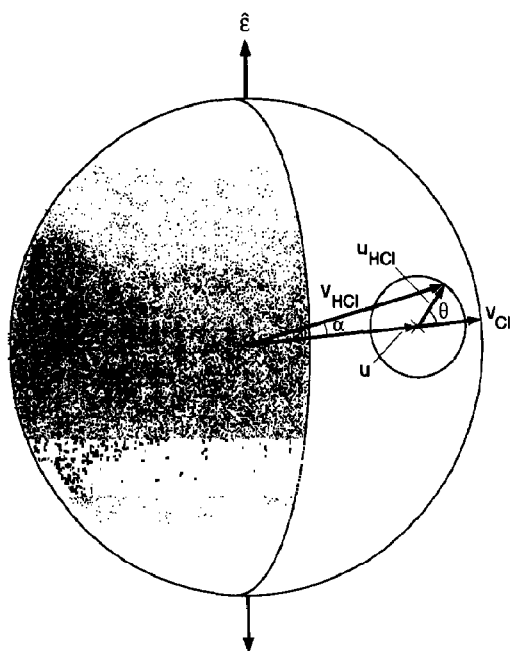


Fig. 3. The kinematics and anisotropy of the reaction: Cl atoms from the 355 nm photolysis of  $\text{Cl}_2$  expand outwards on the surface of a sphere. The shading indicates the probability distribution for  $\beta = -1$ . Inset is a Newton diagram for reaction (1) for a single Cl atom velocity. For the experimental conditions described in section 2, the velocity of the center of mass and the relative velocity lie parallel to the Cl atom velocity.  $\text{HCl}(v' = 1, J')$  is scattered on the surface of the small sphere, with a radius determined by energy conservation. A measurement of  $v_{\text{HCl}}$  determines  $\theta$  because knowledge of the three sides of a triangle determines its angles.

mensional velocity distribution of the HCl product (eq. (10) of ref. [11]), we obtain

$$f(v_{\text{HCl}}) = \sum_{n=1}^N \frac{a_n \delta(v_{\text{HCl}} - v_n)}{4\pi v_{\text{HCl}}^2} \times [1 + \beta P_2(\hat{v}_{\text{HCl}} \cdot \hat{u}) P_2(\hat{v}_{\text{HCl}} \cdot \hat{\epsilon})]. \quad (3)$$

where  $v_n$  is the laboratory frame HCl speed corresponding to a scattering angle  $\theta_n$ , and we have made use of the transformation

$$\delta(v_{\text{HCl}} - v_n) = \delta(\cos \theta - \cos \theta_n) \left| \frac{d \cos \theta}{d v_{\text{HCl}}} \right| = \delta(\cos \theta - \cos \theta_n) \frac{v_{\text{HCl}}}{u_{\text{HCl}} u}. \quad (4)$$

Eq. (3) can be rewritten as

$$f(v_{\text{HCl}}) = \sum_{n=1}^N a_n I_n(v_x, v_y, v_z; u_{\text{HCl}}, \cos \theta_n), \quad (5)$$

where

$$I_n(v_x, v_y, v_z; u_{\text{HCl}}, \cos \theta_n) = \frac{\delta(v_{\text{HCl}} - v_n)}{4\pi v_{\text{HCl}}^2} \times [1 + \beta P_2(\hat{v}_{\text{HCl}} \cdot \hat{u}) P_2(\hat{v}_{\text{HCl}} \cdot \hat{\epsilon})]. \quad (6)$$

The angular form of  $I_n(v_x, v_y, v_z; u_{\text{HCl}}, \cos \theta_n)$  will reflect the anisotropy of the Cl-reagent velocity distribution because the speed of the center of mass is much larger than the speed of the  $\text{HCl}(v' = 1, J')$  product (see fig. 3). In general,

$$\beta_{\text{HCl}} = \langle P_2(\hat{v}_{\text{HCl}} \cdot \hat{u}) \rangle \beta, \quad (7)$$

where  $\beta_{\text{HCl}}$  is the anisotropy parameter for the laboratory-frame distribution of reaction products,  $\beta$  is the anisotropy parameter for the  $\text{Cl}_2$  photodissociation, and  $\hat{v}_{\text{AB}} \cdot \hat{u} = \cos \alpha$ . Because  $\alpha$  is constrained to values  $\leq 18^\circ$  for the product of reaction (1), we note that  $\beta_{\text{HCl}} \approx \beta$ , and thus the angular parts of the  $I_n(v_x, v_y, v_z; u_{\text{HCl}}, \cos \theta_n)$  will reflect the Cl atom anisotropy. We approximate  $f(v_{\text{HCl}})$  in eq. (5) by a summation over eleven functions which are chosen to correspond to eleven scattering angles,  $\theta_n$ , equally distributed in  $\cos \theta$ . We choose  $\cos \theta_n = -10/11, -8/11, \dots, 10/11$  in this procedure. The three-dimensional distribution is projected into the plane containing the TOF and probe laser axes and is then integrated over the probe laser direction with a Doppler resolution function  $D(v_x)$  to give a one-dimensional velocity distribution. We use each of the eleven basis functions in turn,

$$I_n(v_z; u_{\text{HCl}}, \cos \theta_n) = \int dv_y \int dv_x D(v_x) \times I_n(v_x, v_y, v_z; u_{\text{HCl}}, \cos \theta_n). \quad (8)$$

The resultant functions are then convoluted with the instrumental TOF resolution function  $T(v_2)$  to give an experimental signal for each scattering projection  $S_n(v; u_{\text{HCl}}, \cos \theta_n)$ ,

$$S_n(v; u_{\text{HCl}}, \cos \theta_n) = \int dv_2 T(v - v_2) \times I_n(v_2; u_{\text{HCl}}, \cos \theta_n). \quad (9)$$

The forms of these functions will be similar to the double-peaked TOF profiles that arise from  $\text{Cl}_2$  pho-

tolysis because of the near conservation of the photolysis anisotropy (eq. (7)).

The measured experimental signal  $S(v)$  is strictly given by the integral of the product of the differential cross section  $d\sigma/d\Omega$  and the signal functions  $S(v, u_{\text{HCl}}, \cos\theta)$ , but within our approximation of eq. (5), it is given by a summation over the eleven selected values of  $\cos\theta_n$ , weighted by the coefficients  $a_n$ ,

$$S(v) = \sum_{n=1}^{11} a_n S_n(v, u_{\text{HCl}}, \cos\theta_n). \quad (10)$$

The probe laser resolution function,  $D(v_x)$ , is a Lorentzian profile with a fwhm equal to the maximum possible HCl Doppler width, and the TOF resolution function,  $T(v_z)$ , is a 9.5 ns (540 m/s) fwhm Gaussian profile. The TOF data  $S(v)$  are fitted to a linear combination of the functions  $S_1(v, u_{\text{HCl}}, \cos\theta_1)$  to  $S_{11}(v, u_{\text{HCl}}, \cos\theta_{11})$  using a singular-value decomposition (SVD) procedure [31]. During the SVD procedure, the singular-value elements are set to zero if they are less than 5% of the size of the maximum element. This threshold ensures a stable fitting procedure by truncating the fit in the SVD basis set to typically four functions. Without this contraction of the fitting-basis set, instabilities arise because the angular resolution of the eleven-function basis exceeds that of the experimental data.

The SVD-fit coefficients are transformed to the coefficients of eq. (2), and these values are then used to regenerate the differential cross section. Figs. 4 and 5 show the fit and the results of this fitting procedure for two values of  $J'$  of the  $\text{HCl}(v'=1)$  product. We might expect that the TOF profiles would also be sensitive to rotational alignment of the reaction products and other vector correlations [27]. Profiles recorded with horizontal and vertical linear polarizations of the probe laser, were observed to have the same form within experimental uncertainty. This result is probably a consequence of probing on the Q branch of a two-photon  $\Sigma-\Sigma$  transition, which is fairly insensitive to rotational alignment; if desired, we could investigate the alignment of products via alternative spectroscopic transitions.

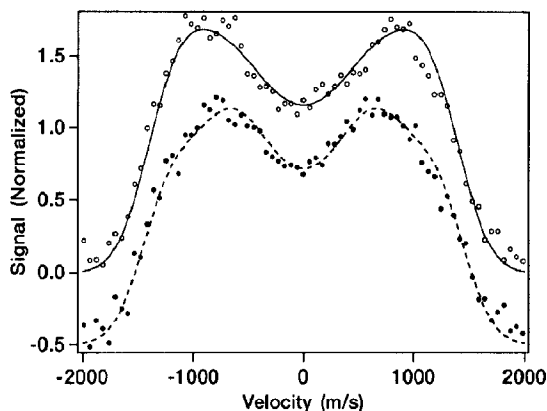


Fig. 4. TOF profiles for (○, —)  $\text{HCl}(v'=1, J'=1)$  and (●, ---)  $\text{HCl}(v'=1, J'=3)$  together with fits to the data (lines) performed as described in the text. For clarity, the central component of the profiles, attributed to energy transfer between  $\text{CH}_4$  and HCl, has been subtracted out. The data are normalized to equal area and are offset vertically.

### 3.3. Background correction

In the fitting procedure, allowance was made for the presence of contaminant HCl in our gas mixture. This contamination of HCl leads to  $\text{HCl}(v'=1)$  molecules via a pathway involving near-resonant energy transfer from  $\text{CH}_4(v_3=1)$ . This background was assigned to this pathway because it depends on the OPO but not on the photolysis laser. Additionally, the background increases approximately linearly with pump-probe time delay and increases when HCl is added to the reaction mix. Its TOF peak is narrow; it is approximately Gaussian with a fwhm of 7.0 ns, which is close to the width of the instrument-resolution function. Thus the HCl product has little kinetic energy, which provides additional evidence for this assignment. In the fitting procedure, a 7.0 ns fwhm Gaussian function centered at the middle of the TOF profile was introduced to account for this contribution to the  $\text{HCl}(v'=1)$  signal.

## 4. Discussion

Traditional experiments for measuring differential cross sections have typically made use of crossed molecular beams and gave rise to the notions of stripping, rebound, and complex-mode reaction

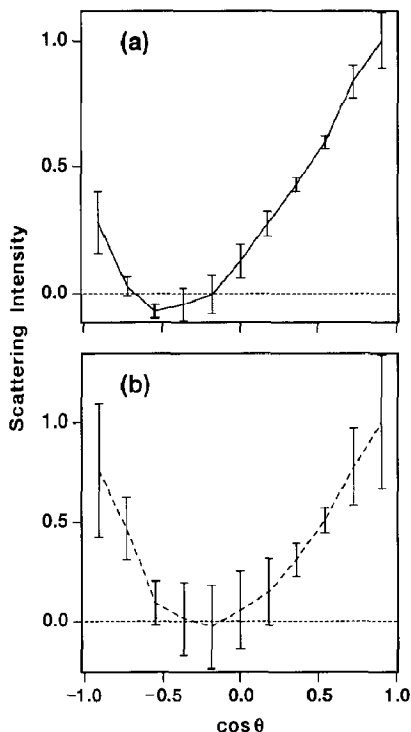


Fig. 5. Extracted differential cross sections for (a)  $\text{HCl}(v'=1, J'=1)$  and (b)  $\text{HCl}(v'=1, J'=3)$  from the reaction  $\text{Cl}(^2\text{P}_{3/2}) + \text{CH}_4(v_3=1, J=1)$  at a center-of-mass collision energy of 0.159 eV. The estimated errors are two standard deviations based on the SVD fitting procedure.

mechanisms [32]. Such experiments were not, however, generally sensitive to the scattering dynamics on a quantum-state-resolved level. Recently, several experimental methods have been developed to measure quantum-state-specific differential cross sections, by making use of techniques such as ion imaging [33–35], one- and two-dimensional Doppler spectroscopy [36], and Rydberg-atom TOF translational spectroscopy [37]. In this study, we have taken the process a step further by measuring product-state-resolved differential cross sections for state-selected reagents. The analysis of the data presented in section 3 provides substantial detail of the dynamics of reaction (1), which would not come from separate measurements of rovibrational state populations and quantum-state-averaged differential cross sections.

Even without the fitting procedure described in

section 3.2, the TOF data demonstrate some interesting effects. Examining the  $J' = 1$  peak, we find significant signal occurs beyond the maximum laboratory-frame projection of the center-of-mass speed. This signal corresponds to forward-scattered  $\text{HCl}(v' = 1, J' = 1)$ , and the fit for this product state confirms that forward scattering is the predominant component of the differential cross section. The fitted differential cross section does, however, go slightly negative in some regions, and we believe this unphysical result is an artifact of the fitting procedure. Possible sources of error include truncation of the fitting expansion or an imprecise TOF-to-velocity conversion calibration. Translational energy release is required to produce speeds greater than the center-of-mass speed, and thus the observed forward scattering requires that the  $\text{CH}_3$  fragment carries little internal energy. Specifically, production of  $\text{HCl}(v' = 1)$  in coincidence with excitation of  $v' = 1$  of the umbrella mode of  $\text{CH}_3$ , which has a frequency of  $606 \text{ cm}^{-1}$ , removes more than 80% of the excess energy of reaction from product translation, and this loss of translational energy is inconsistent with the observed width of the TOF profile. The experimental data therefore imply that for production of  $\text{HCl}(v' = 1)$ , the remaining energy from the reaction is preferentially channelled into product translation as opposed to  $\text{CH}_3$  internal mode excitation.

The reaction dynamics leading to forward-scattered, rotationally cold  $\text{HCl}(v' = 1)$  clearly differ from the interpretation by Andresen and Luntz [18] of the dynamics of the reactions of  $\text{O}(^3\text{P})$  with hydrocarbons. In these systems, the cold-OH product rotational distribution was associated with backward scattering from a linear transition state. Our measurements are, however, consistent with the observations by Flynn and co-workers [38] of translationally hot DCl produced by the reaction of Cl with cyclohexane- $\text{d}_{12}$ .

A simple, impulsive model [39] of the rotational excitation of the products predicts that the deviation from linearity of the Cl–H– $\text{CH}_3$  bond angle in the transition state must take values  $\leq 5^\circ$  for the HCl to be formed in rotational states  $J' \leq 2$ . If the energy release of the reaction is impulsive, this requirement of a near linear transition state can be reconciled with the differential cross section data if we invoke a mechanism that involves the H-atom tracking the

relative motion of the Cl at non-zero impact parameters. Possible origins of this tracking are: (i) C-H bending vibrations, either from the zero-point motion as proposed by Flynn and co-workers [38] for the reaction of Cl with cyclohexane- $d_{12}$ , or in the case of reaction (1) from the  $\nu_3$  mode that we have excited; (ii) rotational motion of the  $\text{CH}_4$  matching the relative tangential speed of the Cl, which has been slowed sufficiently by the barrier to reaction; (iii) a well on the vibrationally adiabatic surface [40] (caused by a suppression of the H-atom vibrational frequency because of the proximity of two heavy atoms) that instills a lifetime to the transition state and thus permits the transition state to rotate as a whole. This last mechanism corresponds quantum mechanically to a dynamical resonance. We would expect mechanisms (ii) and (iii) to be highly sensitive to the collision energy.

An alternative model of the dynamics that is consistent with our data is for the reaction to take place in the non-impulsive limit. If the H-atom transfer is associated with little or no repulsive energy release, the Cl will not be deflected, and the HCl rotation will arise from the relative speed of the H and Cl at the time of transfer. If we assume that the barrier to reaction is equal to the endothermicity of this channel (a lower bound), the relative speed of the Cl and  $\text{CH}_4$  at the barrier is  $1200 \text{ m s}^{-1}$ , which would correspond approximately to  $J' = 2$  of HCl (for which the tangential speed of the rotating H atom is  $1250 \text{ m s}^{-1}$ ). This correspondence supports the idea that nonimpulsive transfer of the H atom from  $\text{CH}_3$  to Cl can result in low rotational excitation, even for Cl-H- $\text{CH}_3$  configurations that are bent at the time of H-atom transfer.

The TOF profile for  $\text{HCl}(v' = 1, J' = 3)$  qualitatively differs from that for  $\text{HCl}(v' = 1, J' = 1)$ . Given that the error bars in fig. 5 represent two standard deviations, the fit to the data for  $\text{HCl}(v' = 1, J' = 3)$  indicates a greater backward-scattering component than for  $\text{HCl}(v' = 1, J' = 1)$  in the differential cross section, although the majority of the product is forward scattered. This result demonstrates that the scattering dynamics are a function of  $J'$  in this system and is an observation that would have been almost impossible to make by either a traditional scattering experiment or a state-resolved integral cross section measurement.

Presently, we are unable to determine unambiguously the mechanism for reaction (1), but further experiments are in progress to clarify our understanding of the nature of the reaction dynamics. We have recently obtained three-dimensional slices of the  $\text{HCl}(v' = 1)$  velocity distribution and the directly extracted differential cross sections are in good agreement with the results presented in this Letter. The observed differential cross sections, and the possible mechanisms suggested here are applicable only to  $\text{HCl}(v' = 1)$  products of reaction (1). We have not yet studied the  $\text{HCl}(v' = 0)$  reaction channel, and hence we can make no assertions about the form of the differential cross section leading to such products. Our results have clearly demonstrated, however, that a great wealth of dynamical information can be obtained by measuring state-to-state differential cross sections and that this goal can be achieved under bulb conditions.

## 5. Conclusion

We have demonstrated the measurement of state-to-state resolved differential cross sections for a reaction conducted in a bulb. We have obtained more information about the reaction of Cl with  $\text{CH}_4$  than is possible by measuring separately either the product-state integrated scattering distribution or the scattering integrated product state distribution. The experiments described in this Letter go a step beyond the degree of detail afforded by a product-state resolved differential cross section by making possible reagent-state dependent studies via laser state preparation. We have shown that the scattering distribution changes as a function of  $J'$  for reaction (1), and we have also found that a cold product rotational distribution is not necessarily correlated with backscattering.

## Acknowledgement

WRS thanks the National Science Foundation for a predoctoral fellowship. This work has been supported by the National Science Foundation under grant No. CHE 89-21198.

## References

- [1] G.W. Flynn and R.E. Weston, *Ann. Rev. Phys. Chem.* 37 (1986) 551.
- [2] G.W. Johnston, S. Satyapal, R. Bersohn and B. Katz, *J. Chem. Phys.* 96 (1990) 206.
- [3] G.E. Hall, 12th Combustion Research Conference, Tahoe City, June 1990 (The Combustion Research Facility of Sandia National Laboratory, Livermore, 1990).
- [4] N.E. Shafer, Ph.D. Thesis, Columbia University (1990).
- [5] F. Green, G. Hancock, A.J. Orr-Ewing, M. Brouard, S.P. Duxon, P.A. Enriquez, R. Sayos and J.P. Simons, *Chem. Phys. Letters* 182 (1991) 568.
- [6] M. Brouard, S.P. Duxon, P.A. Enriquez and J.P. Simons, *J. Chem. Phys.* 97 (1992) 7414.
- [7] M.P. Casassa, D.G. Sauder and D.S. King, *SPIE proceedings* 1858 (1993) 256.
- [8] F.J. Aoiz, M. Brouard, P.A. Enriquez and R. Sayos, *J. Chem. Soc. Faraday Trans.*, in press.
- [9] M. Costen, G. Hancock, A.J. Orr-Ewing and D. Summerfield, *J. Chem. Phys.*, submitted for publication.
- [10] M. Brouard, S.P. Duxon, P.A. Enriquez and J.P. Simons, *J. Chem. Soc. Faraday Trans.*, in press.
- [11] N.E. Shafer, A.J. Orr-Ewing, W.R. Simpson, H. Xu and R.N. Zare, *Chem. Phys. Letters* 212 (1993) 155.
- [12] F.F. Crim, *Ann. Rev. Phys. Chem.* 35 (1984) 657.
- [13] A. Sinha, M.C. Hsiao and F.F. Crim, *J. Chem. Phys.* 94 (1991) 4928.
- [14] M.J. Bronikowski, W.R. Simpson and R.N. Zare, *J. Phys. Chem.* 97 (1993) 2194.
- [15] M.J. Bronikowski, W.R. Simpson and R.N. Zare, *J. Phys. Chem.* 97 (1993) 2204.
- [16] A.R. Ravishankara and P.H. Wine, *J. Chem. Phys.* 72 (1980) 25.
- [17] T.N. Truong, D.G. Truhlar, K.K. Baldrige, M.S. Gordon and R. Steckler, *J. Chem. Phys.* 90 (1989) 7137.
- [18] P. Andresen and A.C. Luntz, *J. Chem. Phys.* 72 (1980) 5842.
- [19] G.E. Busch, R.T. Mahoney, R.I. Morse and K.R. Wilson, *J. Chem. Phys.* 51 (1969) 449.
- [20] Y. Matsumi, K. Tonokura and M. Kawasaki, *J. Chem. Phys.* 97 (1992) 1065.
- [21] W.J. van der Zande, R. Zhang, R.N. Zare, K.G. McKendrick and J.J. Valentini, *J. Phys. Chem.* 95 (1991) 8205.
- [22] T.A. Spiglanin, D.W. Chandler and D.H. Parker, *Chem. Phys. Letters* 137 (1987) 414.
- [23] D.S. Green, G.A. Bickel and S.C. Wallace, *J. Mol. Spectry.* 150 (1991) 303.
- [24] D.S. Green, G.A. Bickel and S.C. Wallace, *J. Mol. Spectry.* 150 (1991) 354.
- [25] D.S. Green, G.A. Bickel and S.C. Wallace, *J. Mol. Spectry.* 150 (1991) 388.
- [26] J.F. Black and I. Powis, *Chem. Phys.* 125 (1988) 375.
- [27] M. Mons and I. Dimicoli, *J. Chem. Phys.* 80 (1989) 4037.
- [28] H.J. Hwang and M.A. El-Sayed, *Chem. Phys. Letters* 170 (1990) 161.
- [29] L.D. Waits, R.J. Horowitz and J.A. Guest, *Chem. Phys.* 155 (1991) 149.
- [30] S. Arepalli, N. Presser, D. Robie and R.J. Gordon, *Chem. Phys. Letters* 118 (1985) 88.
- [31] W.H. Press, B.P. Flannery, S.A. Teukolsky and W.T. Vetterling, *Numerical recipes. The art of scientific computing* (Cambridge Univ. Press, Cambridge, 1986).
- [32] R.D. Levine and R.B. Bernstein, *Molecular reaction dynamics and chemical reactivity* (Oxford Univ. Press, Oxford, 1987).
- [33] M.A. Buntine, D.A. Baldwin, R.N. Zare and D.W. Chandler, *J. Chem. Phys.* 94 (1991) 4672.
- [34] T.N. Kitsopoulos, M.A. Buntine, D.P. Baldwin, R.N. Zare and D.W. Chandler, *Science*, in press.
- [35] A.G. Suits, L.S. Bontuyan, P.L. Houston and B.J. Whitaker, *J. Chem. Phys.* (1992) 8618.
- [36] N.E. Shafer and R. Bersohn, *J. Chem. Phys.* 94 (1991) 4817.
- [37] L. Schnieder, K. Seekamp-Rahn, F. Liedeker, H. Steuwe and K.H. Welge, *Faraday Discussions Chem. Soc.* 91 (1991) 259.
- [38] J. Park, Y. Lee, J.F. Hershberger, J.M. Hossenlopp and G.W. Flynn, *J. Am. Chem. Soc.* 114 (1992) 58.
- [39] H.B. Levene and J.J. Valentini, *J. Chem. Phys.* 87 (1987) 2594.
- [40] I.W.M. Smith, *Accounts Chem. Res.* 23 (1990) 101.